Energy Conversion and Management: X 31 (2026) 102027

Contents lists available at ScienceDirect

Energy Conversion and Management: X

journal homepage: www.sciencedirect.com/journal/energy-conversion-and-management-x

One cell, two commodities: co-producing magnesium and chlorine from waste via molten-salt electrolysis

Alen Rupnik [a,b], Janvit Teržan [a,c], Miha Grilc [a,b], Blaž Likozar [a,*]

[a] Department of Catalysis and Chemical Reaction Engineering, National Institute of Chemistry, Hajdrihova 19, 1000 Ljubljana, Slovenia
[b] Materials graduate study program, University of Nova Gorica, Vipavska 13, 5000 Nova Gorica, Slovenia
[c] Laboratory for demonstration of H_2 and CO_2 technologies, National Institute of Chemistry, Loke pri Zagorju 14 B, 1412 Kisovec, Slovenia

ARTICLE INFO

Keywords:
MSE electrolysis
Magnesium Chloride Electrolysis
Molten salt electrolysis
Magnesium production
Critical raw materials

ABSTRACT

Magnesium is a critical lightweight metal used in aviation, automotive manufacturing, and battery production, but its conventional production remains energy-intensive and carbon-emitting. Molten salt electrolysis (MSE) offers a promising alternative, though challenges related to reactor design, chlorine management, and system stability remain. In this study, a custom-built lab scale molten salt electrolysis reactor (MSER) for $MgCl_2$ electrolysis is developed and experimentally evaluated. The reactor integrates modular graphite electrodes, refractory containment, and a sealed chlorine handling system. Electrolysis at 800 °C and 20 A produced metallic magnesium with an apparent faradaic efficiency of 62.1%, based on recoverable product mass. Electrochemical characterization (CV and LSV) was used to identify the operational voltage window for magnesium deposition and chlorine evolution under two-electrode conditions. Thermal simulation and infrared measurements confirmed stable temperature gradients and safe operation of the reactor head. SEM–EDS analysis confirmed magnesium as the dominant component of the product, with contributions from surface oxidation and minor impurities related to reactor conditions. The results demonstrate the feasibility of the reactor design and highlight key limitations, including magnesium loss through gas-phase transport, which influence product recovery and efficiency. This work provides a basis for further optimization of molten salt electrolysis systems for magnesium production, a critical raw material.

1. Introduction

Magnesium is a high-demand lightweight metal widely utilized in aerospace, automotive, biomedical, and energy sectors due to its exceptional strength-to-weight ratio, recyclability, and casting versatility. Magnesium is the eighth most abundant element in the Earth's crust and is primarily found in minerals like magnesite ($MgCO_3$) and dolomite ($MgCa(CO_3)_2$) [1]. One of the most promising approaches for magnesium production is molten salt electrolysis (MSE) of magnesium chloride ($MgCl_2$), which can be derived from thermal processing of magnesium oxide (MgO) or directly from waste-based sources [2]. During electrolysis, magnesium ions are reduced at the cathode, while chlorine gas evolves at the anode. Although the Pidgeon process remains dominant in industry, it is energy-intensive and emits 20–50 kg CO_2 per kg of Mg [3], significantly more than aluminium or iron production, and relies on energy-intensive calcination and reduction, making the case for more sustainable electrochemical alternatives increasingly urgent. In contrast, molten salt electrolysis (MSE) offers a more sustainable and lower-carbon route. Another promising source of magnesium is waste sludge from chromium mining and processing, where both magnesium and chromium can be efficiently recovered from oxide- and chloride-bearing residues through molten salt electrolysis. [4–6].

In molten salt electrolysis, magnesium chloride is decomposed into magnesium metal and chlorine gas at high temperatures, typically above 700 °C. The thermodynamics and kinetics of this process are influenced by various factors including the composition of the molten salt, the cell design, and the operating conditions [7,8]. Recent studies have focused on improving the current efficiency and reducing energy consumption by optimizing these parameters [9].

Conventional processes using anhydrous $MgCl_2$ are operated at 655–720 °C and reduce emissions (to ~ 5–9 kg CO_2/kg Mg), but still produce toxic chlorine gas and require complex feedstock preparation [10,11]. More recent advances have shifted toward the electrolysis of MgO, which requires higher energy input due to the stronger Mg–O

* Corresponding author.
E-mail addresses: alen.rupnik@ki.si (A. Rupnik), janvit.terzan@ki.si (J. Teržan), miha.grilc@ki.si (M. Grilc), blaz.likozar@ki.si (B. Likozar).

https://doi.org/10.1016/j.ecmx.2026.102027
Received 14 January 2026; Received in revised form 5 May 2026; Accepted 1 June 2026
Available online 2 June 2026

bond compared to Mg–Cl complexes. Most of this conversion is conducted in fluoride-based molten salts [12] (e.g., MgF_2–CaF_2 or MgF_2–LiF systems), which eliminates Cl_2 emissions and allows direct reduction of the oxide feedstock. For example, a study by Armaghan E. T. et al. [13], investigated the effects of using a liquid tin cathode to improve the electrolysis efficiency. They found that the current yields measured in this study were the highest for electrolytic MgO reduction in molten MgF_2-CaF_2 salt, at 94–97% for carbon anodes and 84% for YSZ-SOM anodes. This improvement is likely due to the reactive nature of the tin cathode, which lowers the activity of the magnesium product—thereby increasing the reduction driving force and reducing both metallic Mg dissolution and electronic conductivity in the electrolyte. However, such systems raise concerns regarding product purity and the potential migration of fluorine from the melt. Liquid metal cathodes more broadly have been shown to offer several advantages over solid counterparts, including enhanced depolarization effects, reduced energy consumption, and improved resistance to product oxidation and dissolution [14,15,16]. The lowered activity of magnesium in such cathodes shifts the reduction potential, increasing the driving force and promoting higher current efficiency while suppressing back-diffusion into the electrolyte [17].

Despite these promising developments, the majority of existing research relies on conventional, commercially available electrochemical cells that are also more manageable in non-corrosive industrial setups. Despite the electrochemical promise of MSE, much of the literature relies on legacy reactor platforms. There is a need for modular, corrosion-resistant systems that allow tighter control over variables like electrode spacing, gas collection, and thermal gradients [18,19,20]. Design variables such as salt composition, containment materials, temperature control, and electrode configuration have not been sufficiently explored, especially with regard to scalable or customisable reactors tailored to the MSE of magnesium chloride or oxide salts [21,22]. Furthermore, environmental aspects have driven research to reduce the carbon footprint of magnesium production. Moreover, the release of toxic chlorine gas during the electrolysis process poses both environmental and safety challenges, necessitating the development of effective capture and utilization strategies [23]. Chlorine evolution is often unavoidable in chloride-based MSE, and its accumulation or leakage can pose operational hazards or environmental liabilities [24,25].

To address this gap, we present the development and testing of an in-house-built molten salt electrolysis reactor (MSER), specifically engineered for magnesium production from anhydrous $MgCl_2$. The system includes a custom-fabricated PTFE gas outlet connected to a NaOH-based chlorine scrubbing system, assembled from chemically resistant PVC-C components and linked via PTFE tubing to ensure compatibility with warm chlorine gas. The reactor features a graphite crucible serving as the cathode, a central graphite rod as the anode, and a sealed quartz and alumina combo headspace designed to safely manage chlorine evolution. This design prioritizes modularity, precise thermal control, and high chemical durability through the use of advanced refractory materials such as high-purity alumina (DEGUSSIT 23) and graphite.

It should be noted that, while this study is motivated by the valorisation of magnesium-rich industrial residues within the EU-Magnesium project, the present work focuses on reactor development and validation using commercially available anhydrous $MgCl_2$. The use of pure feedstock enables controlled evaluation of reactor behaviour and electrochemical performance without additional complexity from impurities. Electrolysis of waste-derived $MgCl_2$ will be addressed in subsequent studies.

2. Experimental

The primary contribution of this work is the design and experimental validation of a laboratory-scale molten salt electrolysis reactor, with a focus on safe chlorine handling, modular configuration, and identification of key limitations governing magnesium recovery and efficiency.

2.1. Molten salt reactor design

For the batch experiments, we used an electrolytic molten salt reactor (MSER) that we developed and built ourselves (Fig. 1). The reactor consists of a stainless-steel housing and a graphite crucible that serves a dual purpose: it holds the molten salt and serves as a cathode and a reaction vessel. The crucible is sealed with a chlorine-resistant quartz cover, which has an opening that enables the insertion of the alumina tube. The latter descends to the reactor core and is connected to a PTFE top fitting, allowing for the purging of chlorine gas and the insertion of the graphite anode into the reactor. The gap between the electrodes is maintained at 5 mm.

The chlorine outlet is connected to a series of four PVC-C scrubber tubes filled with 5 wt.% NaOH(aq.), which neutralizes the chlorine gas produced. A sampling valve is located upstream of the scrubber system to facilitate the monitoring of chlorine formation (see Chapter 2.3). The electrodes are connected to a potentiostat, which serves both as a power source and as an electroanalytical instrument (see Chapter 2.2). The reactor core is located within a vertical tube furnace, specifically manufactured by Thermansys.

The experiment was carried out at 800 °C, which was measured inside the reactor with a K-type thermocouple positioned at about the middle of the melt. The furnace temperature was set to 900 °C to reach and maintain the desired internal temperature. The reaction was run for 2 h at a constant current of 20 A, with the applied voltage between 7.5 to 9.0 V at this current. Throughout the experiment, the reactor was continuously purged with an argon flow of 10 mL/min to maintain an inert atmosphere and prevent unwanted corrosion. In this study, commercially sourced anhydrous $MgCl_2$ ($\geq$98%) was used to evaluate reactor performance under controlled conditions. In parallel, waste-derived $MgCl_2$ is being developed and will be employed in subsequent

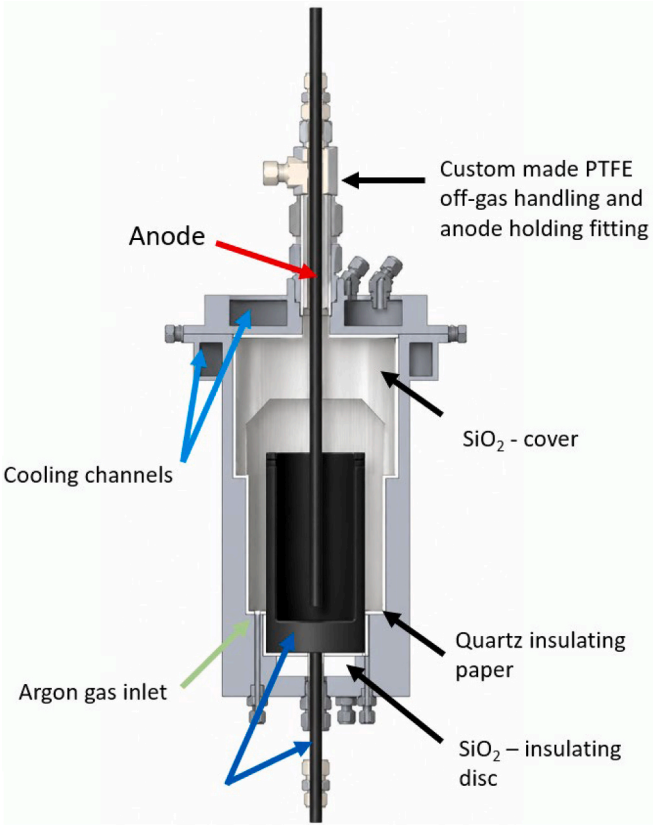

Fig. 1. CAD model of the custom molten salt electrolysis (MSE) cell showing the anode, cathode crucible, SiO_2 cover, quartz paper insulation, SiO_2 disc barrier, cooling channels, and argon gas inlet.

electrolysis experiments as part of ongoing EU-Magnesium project. While industrial processes often use eutectic mixtures (e.g., $MgCl_2$–NaCl or $MgCl_2$–$CaCl_2$) to lower the melting point and enhance conductivity, the present study aimed to establish a performance baseline using pure $MgCl_2$. Future experiments will incorporate eutectic systems to evaluate their influence on reactor efficiency and product handling.

2.2. Electroanalytical measurements

We used the potentiostat SP-150 from Biologic, together with a 20 A Booster as the power supply and as an electroanalytical instrument. To confirm the reaction at the electrodes, we performed cyclic voltammetry (CV) to determine reduction and oxidation peaks. Chronopotentiometry was used for the experiment, where we set the current to a constant value of 20 A, and measured the potential applied to the electrode in volts (V). The reference connectors were connected to the counter electrode (graphite crucible cathode). As this was a two-electrode configuration, the potential values reflect the voltage between the graphite anode (working electrode) and graphite crucible cathode (counter electrode), and not vs. an independent reference electrode.

2.2.1. Chlorine formation

Chlorine formation was qualitatively confirmed using wetted litmus paper, which exhibits a colour change in the presence of acidic gases. Upon exposure to the reactor off-gas, the litmus paper shifted to orange–red tones, indicating the presence of chlorine. While this method provides a simple and effective means of confirming chlorine evolution and validating the operation of the gas handling system, it remains qualitative and non-specific.

2.3. SEM/EDS analysis

After the experiment, the product collected from the graphite crucible was analysed in detail using a scanning electron microscope (SEM), specifically the HR-SEM Zeiss Supra 35 VP from Carl Zeiss. Small samples, each only a few square millimetres in size, were carefully removed and mounted on a sample holder for examination. The surface morphology of these samples was carefully scanned and their material composition was analysed using an energy dispersive X-ray detector (EDS) integrated into the SEM. Prior to SEM/EDS analysis, the samples were mechanically cross-sectioned, and the measurements were performed on the exposed internal surfaces. This approach minimizes the influence of surface oxidation and provides a more representative assessment of the bulk composition of the electrochemically produced material.

3. Results

3.1. Molten salt reactor setup

The custom designed molten salt electrolysis reactor (MSER) is shown in Fig. 2. The system successfully maintained operational stability during the electrolysis experiments, with all safety and monitoring subsystems functioning as designed. The vertical tube furnace ensured uniform heating of the graphite crucible, while the cooled reactor head allowed integration of PTFE tubes for handling the chlorine containing exhaust gases.

To evaluate the thermal management in the upper part of the reactor, a SolidWorks finite element simulation was performed to predict the steady-state temperature distribution (Fig. 3.A). The thermal simulation was conducted under steady-state conditions. The reactor walls were subjected to an external convection coefficient of 5 $W/m^2 \cdot K$ to represent natural cooling in ambient air. A fixed temperature of 1073 K was applied to the lower crucible region to mimic furnace heating. Emissivity values of 0.80 (graphite) and 0.75 (alumina) were assigned to the respective surfaces. The results showed a steep axial gradient between the high-temperature crucible region (> 1000 K) and the cooled reactor head (< 400 K). This gradient confirmed that the upper part remained sufficiently cool to allow the safe use of PTFE fittings without exceeding their thermal stability limit.

The simulation also showed that the majority of the thermal load is confined to the lower reactor zone, minimizing heat transfer toward the chlorine outlet. This design ensures both effective electrolysis conditions in the crucible and safe handling of the chlorine at the reactor head. These results validate the proposed design approach and provide a predictive framework for optimizing cooling strategies in subsequent reactor iterations.

This experimental confirmation shows that the cooling of the reactor head is well below the thermal stability threshold of the PTFE components, ensuring safe handling of the chlorine exhaust gas stream. The strong correlation between the simulated and observed temperature profiles underpins the reliability of the prediction of the thermal model and emphasises the suitability of the reactor design for long-term operation.

The selection of graphite for the crucible and electrodes is consistent with established molten salt electrolysis systems due to its high thermal stability, chemical resistance to chloride melts, and electrical conductivity. The stainless-steel housing serves only as a structural containment component and is not intended to be in direct contact with the molten electrolyte. However, under prolonged operation and insufficient chlorine removal, secondary corrosion effects in the upper reactor region may occur. This limitation is further discussed in Section 4 and represents a key design consideration for future reactor iterations.

The simulation is intended as a qualitative engineering tool to assess temperature gradients and safe operation of the reactor head, rather

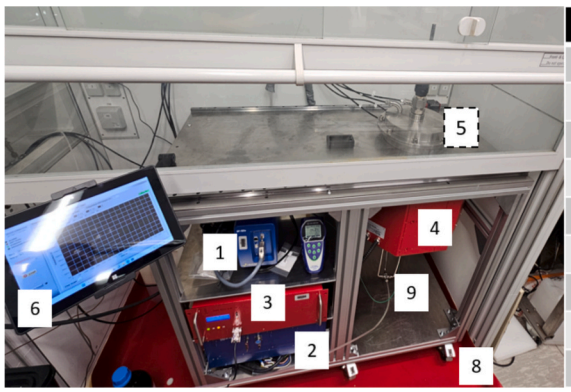

n°	COMPONENTS
1	Potentiostat SP-150
2	20 A Potentiostat Booster
3	Furnace Power Supply
4	Furnace
5	MSE Reactor Unit
6	Furnace Control Tablet
7	Aluminium Profile Frame
8	Smelting Safety Carpet
9	Argon Inlet

Fig. 2. Experimental setup of the in-house built molten salt electrolysis reactor (MSER).

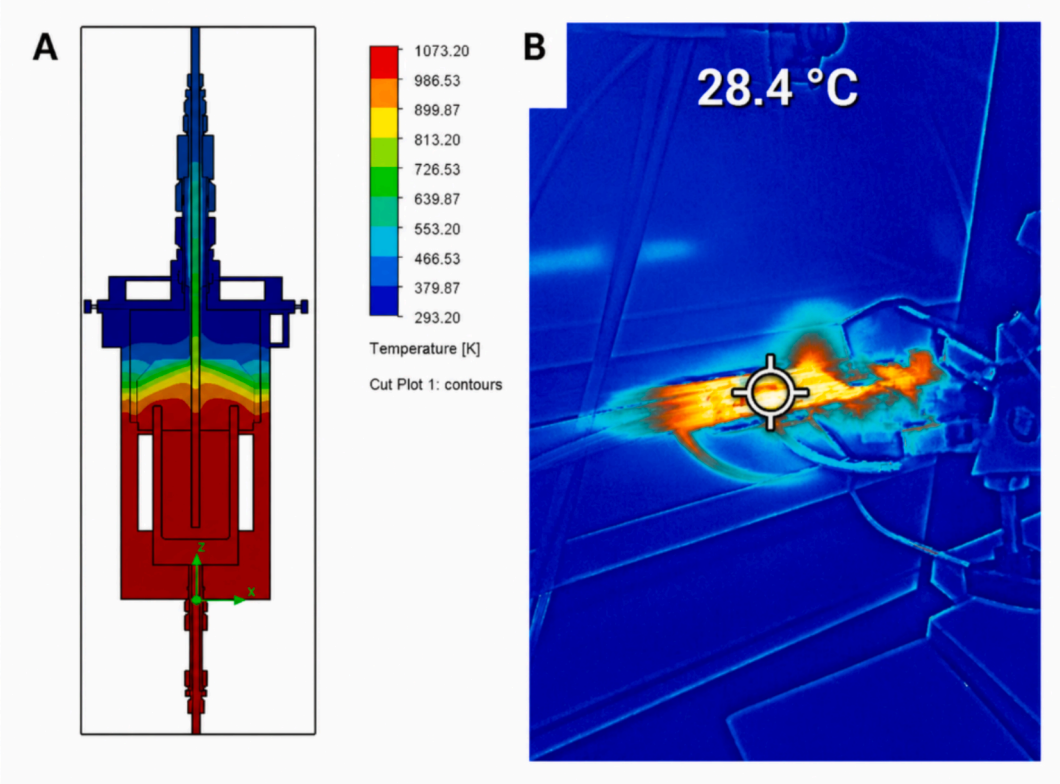

Fig. 3. A: SolidWorks simulation of steady–state temperature profile, showing axial gradient between the molten salt zone and cooled reactor head; 2.B: Infrared thermographic (FLIR) image of the reactor head during electrolysis, showing effective cooling with surface temperatures maintained near 28 °C. Simulation assumes steady-state conditions with external convection (5 W/m^2·K) and emissivity values of 0.80 for graphite and 0.75 for alumina.

than a fully validated Multiphysics model.

3.2. Magnesium production

Electrolysis of anhydrous magnesium chloride ($MgCl_2$) was successfully carried out in the custom-built molten salt reactor. The performance of the system was evaluated in terms of magnesium production, stability of operating conditions, electrode behaviour, and the integrity of reactor components under high-temperature electrolysis conditions.

The experiment was conducted for 2 h at a constant current of 20 A and a temperature of 800 °C. The initial cell potential was 5.6 V, gradually increasing to 6.06 V by the end of the experiment (Fig. 4). This progressive increase is attributed to the formation of chlorine gas at the anode and the concomitant depletion of magnesium chloride in the electrolyte. It is anticipated that enhanced melt mixing could mitigate the rise in potential by maintaining a more uniform electrolyte composition.

Notably, a transient drop in cell potential was observed at approximately 40 min into the experiment, where the voltage decreased to ~ 2.6 V for a duration of ~ 50 s. This phenomenon is likely associated with the formation of a conductive metallic magnesium bridge between the anode and cathode, which temporarily reduced the system resistance. Such behaviour suggests that reducing the electrode spacing may lower the steady-state operating voltage, potentially approaching the target of ~ 6.0 V.

Based on the applied current and reaction time, the theoretical magnesium yield was calculated using Faraday's law of electrolysis:

$$m = \frac{Q^*M^*FE}{Z^*F}$$

Where m is mass of magnesium produced, Q is the total charge passed, M is molar mass magnesium, FE is the faradaic efficiency, Z is number of electrons transferred and F is Faraday's constant with value of 96,500 As/mol. Assuming a representative faradaic efficiency of 80%—consistent with values typically reported for molten salt electrolysis systems (70–90%)—the theoretical magnesium yield is:

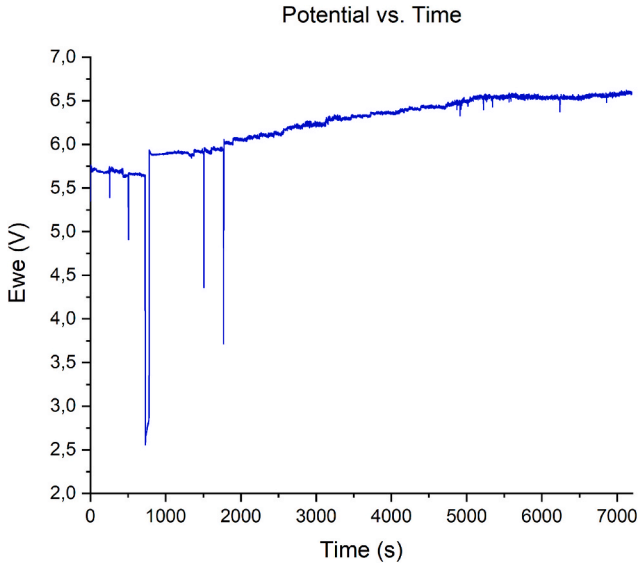

Fig. 4. Chronoamperometric curve of molten $MgCl_2$ electrolysis at constant current over a 2-hour period. The gradual increase in cell voltage reflects system polarization and electrolyte depletion, while transient voltage drops are attributed to magnesium bridging or localized shorting between electrodes.

$$m = \frac{20A*7200s*24.3\frac{g}{mol}*0.8}{2*96500\frac{As}{mol}} = 14.5g$$

Based on the total charge passed, the theoretical magnesium yield at 100% faradaic efficiency was calculated as 18.2 g. After the experiment, the recovered magnesium product weighed 11.3 g. This corresponds to a faradaic efficiency of approximately 62.1%. This value should be considered an apparent efficiency, as it reflects only the collected product and does not account for material losses during operation. Post-experimental inspection of the reactor revealed visible magnesium condensation on cooler surfaces above the crucible, indicating that a fraction of the produced magnesium was transported out of the molten phase and not recovered. These observations suggest that the measured FE is influenced by system-specific transport phenomena, including vapor-phase migration and deposition, which reduce the measurable product yield. As these losses were not quantitatively captured, the reported efficiency represents a lower-bound estimate of the true electrochemical performance of the system. Future improvements such as enhanced electrolyte mixing, crucible impregnation, reduced electrode spacing, and optimized gas removal are expected to increase the faradaic efficiency toward the industrial benchmark.

$$FE = \frac{m*Z*F}{Q*M} = \frac{11.3g*2*96500\frac{As}{mol}}{20A*7200s*24.3\frac{g}{mol}}*100\% = 62,1\%$$

3.3. Cyclic voltammetry and linear sweep potentiometry

Cyclic voltammetry (CV) was employed to investigate the electrochemical behaviour of the molten $MgCl_2$ system under operating conditions relevant to electrolysis. Voltammograms were recorded over a wide potential window of − 6.0 V to + 6.0 V, with the potential measured between the graphite anode and graphite crucible cathode in a two-electrode configuration. The purpose of this wide scan range was to capture the full electrochemical window of the melt and identify the onset of cathodic magnesium deposition and anodic chlorine evolution and the results are shown in Fig. 5. Before CV measurements we measured OCV between the electrodes, and we measured 0.055 V.

The observed cathodic and anodic features do not represent a classical reversible redox couple, but rather two independent electrode processes occurring simultaneously in the molten salt. The cathodic response near − 2.3 V corresponds to the reduction of Mg^{2+} ions to metallic magnesium, while the anodic feature near + 1.6 V is associated with chlorine gas evolution from chloride ions. These reactions are inherently irreversible and occur at different interfaces with significant overpotentials, especially under high-temperature conditions and in the absence of a reference electrode.

Because the system operates in a two-electrode configuration, the measured potentials represent the full cell voltage, including ohmic drops, polarization effects, and gas evolution resistance. Therefore, the separation between anodic and cathodic features cannot be interpreted as a peak separation of a single redox couple, but rather reflects the combined electrochemical and resistive behaviour of the molten salt cell.

Repeated cycling showed consistent features in the voltammograms, indicating stable electrochemical behaviour of the $MgCl_2$ melt and confirming that magnesium deposition and chlorine evolution are the dominant electrode processes within the operating voltage range of the reactor. The CV results should therefore be interpreted as indicative of the operational electrochemical window of the system rather than precise thermodynamic potentials.

Linear sweep voltammetry was performed to further characterize the electrochemical behaviour of the $MgCl_2$ molten salt system (Fig. 6). As with the CV measurements, the potential was recorded in a two-electrode configuration between the graphite anode and graphite crucible cathode, and therefore represents the full cell voltage including ohmic and polarization contributions. The LSV curve shows a gradual increase in current with increasing applied potential, followed by a more pronounced rise beyond approximately 3.0 V. This behaviour reflects the increasing rate of anodic chlorine evolution as the driving force for oxidation increases. The initial current rise near ~ 1.6 V is associated with the onset of chlorine gas formation at the anode, while the cathodic process of magnesium deposition occurs simultaneously at the opposing electrode.

It is important to note once again that these features do not correspond to classical reversible redox peaks, but rather indicate the operational electrochemical window of the molten salt system under real electrolysis conditions. The observed current response is influenced by gas evolution, electrode polarization, melt resistivity, and the absence of a reference electrode, all of which contribute to the shape of the LSV profile.

Together with the CV results, the LSV measurements confirm that magnesium deposition and chlorine evolution are the dominant electrode processes within the applied voltage range and validate the stable

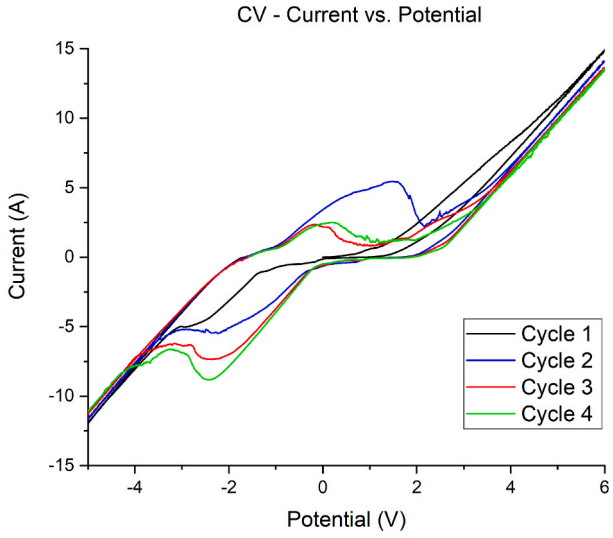

Fig. 5. Cyclic voltammetry of molten $MgCl_2$ recorded in a two-electrode configuration, showing the onset of magnesium deposition at the cathode and chlorine evolution at the anode. Potentials represent full cell voltage between graphite electrodes.

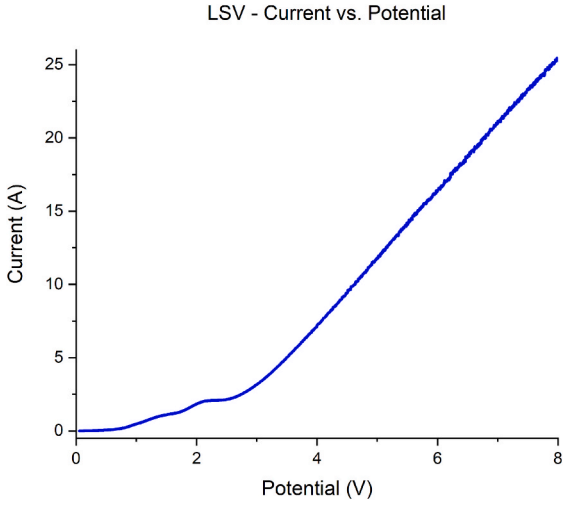

Fig. 6. Linear sweep voltammetry (LSV) of molten $MgCl_2$, showing a sharp increase in anodic current above ~ 1,6 V, consistent with chlorine evolution. Scan rate of LSV was 100 mV/s. Potential is measured against graphite crucible cathode.

operation of the reactor under the investigated conditions.

3.4. Chlorine formation

The presence of chlorine gas in the off-gas stream was qualitatively confirmed using pH-sensitive litmus paper. During electrolysis, exposure of the litmus strips to the reactor off-gas resulted in a pronounced colour transition from sage green to orange and subsequently dark red (Fig. 7). This change is characteristic of strong acidic conditions and provides qualitative evidence of chlorine formation during the electrolysis of magnesium chloride. While this approach confirmed chlorine evolution and validated the functionality of the scrubbing system, it remains qualitative and does not provide information on the quantity or efficiency of chlorine capture. Future work will incorporate quantitative analysis methods, such as iodometric titration of the NaOH scrubbing solution, spectrophotometric determination of hypochlorite and chloride species, and gas-phase flow measurements to establish a complete mass balance of chlorine production and capture efficiency.

3.5. Scanning microscopy and elemental analysis

The reaction product recovered from the graphite crucible was analysed using Scanning Electron Microscopy (SEM) coupled with Energy Dispersive X-ray Spectroscopy (EDS) to evaluate morphology, elemental composition, and possible impurities. The EDS analysis (Fig. 8, Fig. 9 and Table 1) revealed that the sample is composed predominantly of magnesium (~79.4 wt.%), confirming successful electrochemical reduction of Mg^{2+} ions. Oxygen was detected at ~ 16.1 wt. %, which is attributed to surface oxidation and the formation of a thin MgO passivation layer upon exposure to ambient air. A small chlorine content (~1.9 wt.%) indicates the presence of $MgCl_2$ residues, consistent with visual observations of recrystallized salt in the crucible.

In addition to these main constituents, traces of iron (~2.1 wt.%), cobalt, and nickel were detected, which can be attributed to corrosion of the stainless-steel reactor housing. The presence of these transition metals indicates that the purging with argon at a rate of 10 mL/min was not sufficient to prevent the accumulation of chlorine in the reactor headspace, leading to localized corrosion of the stainless-steel components. To mitigate this problem, an increased argon flow rate (50–100 mL/min) is recommended for future experiments to ensure effective chlorine removal and minimize corrosion. Aluminium and carbon were also observed, originating from the SEM sample holder and the carbon tape, respectively, and are not considered part of the electrolysis product.

A representative spherical particle obtained from the crucible after the reaction is presented in Fig. 10. Since the experiment was not aimed at complete $MgCl_2$ conversion, residual salt was also present in the crucible after the reaction.

The quantitative EDS results are summarized in Table 1. They confirm the dominance of magnesium in the product and support the operating performance of the molten salt electrolysis reactor.

The oxygen content detected by EDS is attributed primarily to rapid surface oxidation of magnesium during sample preparation and handling in ambient atmosphere, and does not reflect the bulk composition of the electrochemically produced material.

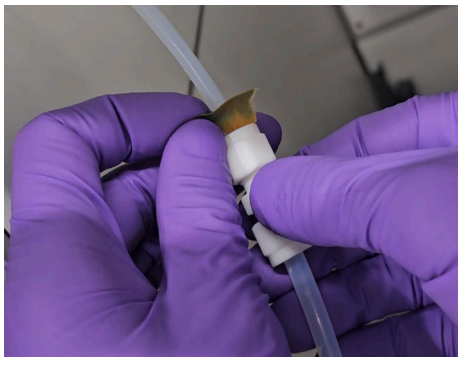

Fig. 7. Discoloration of wet litmus paper when exposed to off-gas stream, corroborating the presence of chlorine gas.

4. Discussion

The behaviour of the system during electrolysis is governed not only by electrochemical reactions at the electrodes, but also by coupled transport and phase phenomena within the reactor. In particular, the high operating temperature (~800 °C) promotes partial vaporization of magnesium, enabling its migration away from the cathodic region and subsequent condensation on cooler surfaces. This introduces a decoupling between electrochemical production and physical recovery of the product, which directly impacts the apparent faradaic efficiency. Similarly, chlorine evolution at the anode contributes to local changes in composition and gas-phase transport, influencing both polarization behaviour and material stability in the reactor headspace.

The faradaic efficiency (FE) of the electrolysis process was calculated to be 62.1%, which is below the typical range of 70–90% reported for molten salt electrolysis systems. Post-experimental inspection of the reactor revealed visible condensation of magnesium on cooler surfaces above the crucible (Fig. 11.B), indicating that a portion of the produced magnesium was transported out of the molten phase and not recovered. Due to deposition on irregular reactor surfaces and within the porous graphite structure, accurate quantification of this lost material is not feasible. Therefore, the faradaic efficiency reported in this study is based solely on the recoverable magnesium mass and represents a lower-bound estimate of the true electrochemical efficiency. This distinction reflects the limitation of mass balance closure in the current reactor configuration. As shown in Fig. 11.A, argon was introduced at the bottom of the reactor to flush chlorine gas and prevent contact with the stainless-steel housing. This upward argon flow, combined with the inherent porosity of the graphite crucible, created pathways for magnesium vapor and fine particles to escape from the molten salt crucible.

A prolonged 16-hour electrolysis test was also conducted to explore long-term stability; however, current instability was observed beyond the 8-hour mark, likely due to magnesium bridging between electrodes. These events caused short circuits and voltage fluctuations, limiting the reliability of the extended run. Future work will focus on reactor design modifications to enable sustained operation with stable faradaic efficiency and reproducible electrolysis conditions. Additional future improvements should also aim to minimize magnesium mobility by using crucibles with lower porosity or protective outer coatings, redesigning argon flow channels to avoid direct upward flows along crucible walls, and incorporating condensation traps or cold fingers to capture volatilized magnesium for post-process quantification. These modifications should significantly reduce magnesium losses, allow a more accurate determination of the reactor's faradaic efficiency and improving overall material recovery.

The geometry and configuration of the reactor were selected to balance compactness, thermal stability, gas separation, and ease of modular assembly. The crucible acts as the cathode and was sized to fit within a standard furnace while maintaining sufficient electrolyte volume for stable operation. The central graphite anode was placed 5 mm from the crucible wall to minimize voltage losses while avoiding short-circuit risk due to magnesium deposition or bridging.

The vertical orientation of the cell allows natural stratification to help separate chlorine and magnesium gases, with evolved Cl_2 being directed into a sealed scrubbing system. The placement of thermocouples and the simulated temperature field ensure that the melt remains fully molten during operation. While flow and electric field uniformity were not yet modelled, the current layout serves as a baseline design for future Multiphysics optimization.

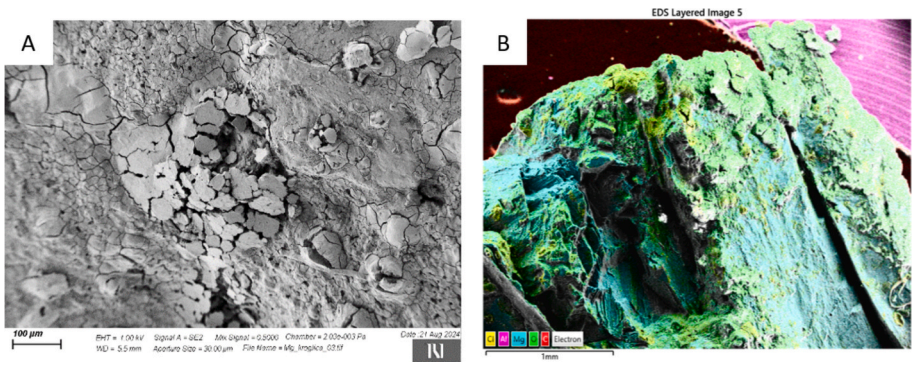

Fig. 8. A: SEM micrograph of spherical magnesium particle produced via electrolysis in the molten salt electrolysis reactor (MSER); B: SEM-EDS elemental mapping of the product sphere.

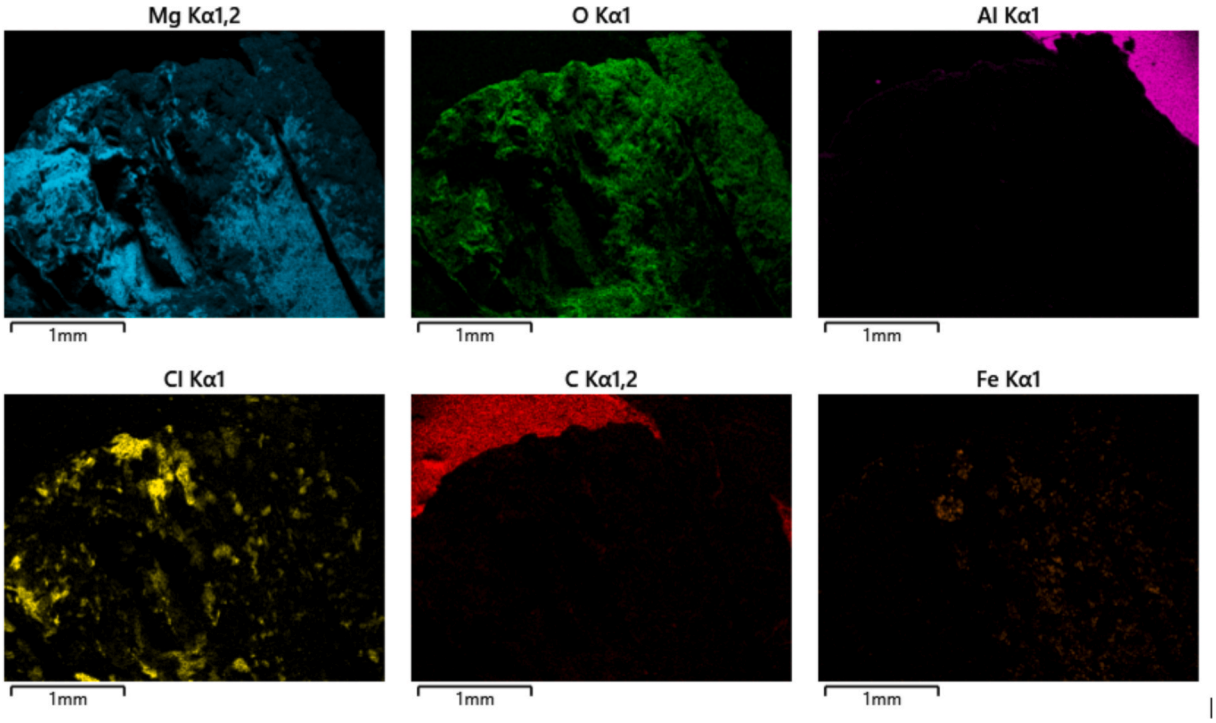

Fig. 9. EDS mapping results. Top row: magnesium, oxygen, and aluminium holder; bottom row: chlorine, carbon tape, and iron signals from stainless-steel reactor housing.

Table 1
Quantitative EDS results of the electrolysis product.

Element	Fraction [Wt.%]
O	16,14
Mg	79,41
Cl	1,88
Ti	0,49
Fe	2,08
Total	**100**

While the fundamental electrochemical configuration (graphite electrodes in molten $MgCl_2$) is consistent with conventional laboratory systems, the present reactor introduces several important engineering advancements. These include a fully integrated chlorine handling system based on a sealed PTFE outlet and multi-stage NaOH scrubbing, enabling safe management of toxic Cl_2 gas. In addition, the use of a machinable quartz cover and sealed alumina headspace improves gas containment and corrosion resistance, while the top-mounted electrode configuration allows modular assembly and easier system access. These features distinguish the reactor from typical laboratory setups, where gas handling and system sealing are often simplified or externally managed. The design therefore provides a more controlled and safer platform for investigating molten salt electrolysis under realistic operating conditions.

5. Conclusion

This study demonstrated the successful design, construction, and operation of a proprietary molten salt electrolysis reactor (MSER) for magnesium chloride electrolysis. Stable reactor performance was achieved, with effective chlorine management demonstrated by both simulation and infrared thermography. Electrochemical analyses confirmed the expected redox processes for magnesium deposition and chlorine evolution, while SEM–EDS characterization confirmed the formation of metallic magnesium with moderate apparent purity, affected by surface oxidation during post-processing and minor contamination from reactor components. The experimental faradaic

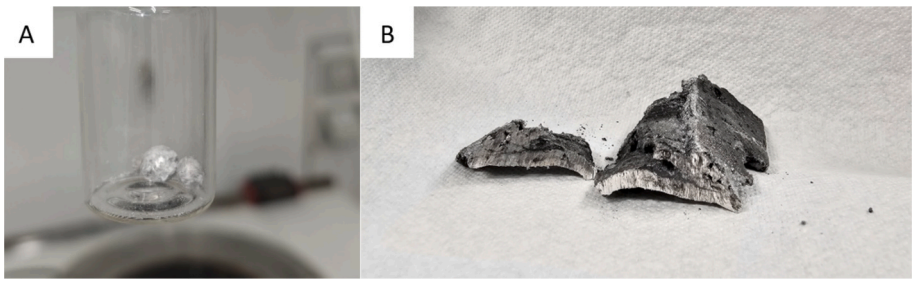

Fig. 10. Representative spherical (figure A) product and large piece (figure B) of product recovered from the graphite crucible.

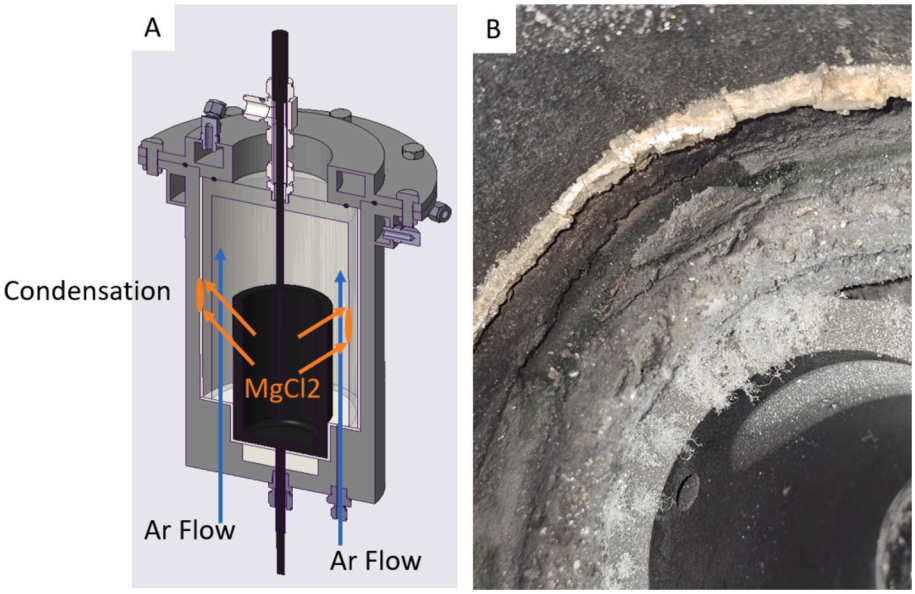

Fig. 11. A: Reactor schematic showing argon purge configuration. 7.B: Photograph of the reactor after the experiment showing condensed magnesium and ferrous-chlorine deposits above the crucible, which is evidence of magnesium loss during electrolysis.

efficiency was calculated to be 62.1%, which is below industry benchmarks. On the other hand, examination of the reactor after the experiment revealed that magnesium losses due to the porosity of the crucible and argon-induced mobility probably led to an underestimation of the actual efficiency.

Future work should focus on minimizing magnesium losses through the use of low-porosity crucibles, optimized argon flow configurations, and the incorporation of condensation traps for volatilized magnesium. These improvements are expected to enhance faradaic efficiency, improve material recovery, and mitigate corrosion within the reactor. In addition, future studies should implement quantitative chlorine detection methods to accurately evaluate gas evolution, capture efficiency, and environmental impact. Overall, the present results demonstrate the feasibility of the MSER and provide a foundation for further optimization and potential scale-up of molten salt electrolysis for magnesium production.

CRediT authorship contribution statement

Alen Rupnik: Writing – review & editing, Writing – original draft, Visualization, Methodology, Investigation, Data curation, Conceptualization. **Janvit Teržan:** Writing – review & editing, Supervision, Formal analysis, Data curation. **Miha Grilc:** Supervision, Project administration. **Blaž Likozar:** Supervision, Project administration, Funding acquisition.

Declaration of competing interest

The authors declare that they have no known competing financial interests or personal relationships that could have appeared to influence the work reported in this paper.

Acknowledgements

This work was supported by the Slovenian Research and Innovation Agency (core funding P2–0152), the European Institute of Innovation and Technology (EIT) RawMaterials project EU-Magnesium, and the European Union's NextGenerationEU program through the HyBReED project.

Data availability

The data supporting the findings of this study are not publicly available due to the ongoing nature of the EU-Magnesium project and institutional data policies. However, the data can be made available by the corresponding author upon reasonable request. All relevant experimental results, figures, and supporting documentation are included within the manuscript and supplementary material.

References

[1] "(PDF) Approaches to High-grade Sintered Magnesia from Natural Magnesite." https://www.researchgate.net/publication/351873286_Approaches_to_High-grade_Sintered_Magnesia_from_Natural_Magnesite (accessed Sep. 01, 2023).

[2] Yuan Y, Li W, Chen H, Wang Z, Jin X, Chen GZ. Electrolysis of metal oxides in MgCl2 based molten salts with an inert graphite anode. Faraday Discuss Aug. 2016; 190:85–96. https://doi.org/10.1039/C5FD00231A.
[3] Shi H, et al. Direct molten-salt electro-reduction of CO2 in porous electrodes. Chem Eng J 2023;vol. 462, no. January:142240. https://doi.org/10.1016/j.cej.2023.142240.
[4] "Project Eu Magnesium". (accessed Sep 2022;12:2025). https://muresmag.eu/project-eu-magnesium/.
[5] B. Feng, Y. Jia, J. An, Y. Jia, and M. Wang, "Clean preparation of Cr2O3 by direct molten salt electrolysis of sodium chromate," *J. Clean. Prod.*, vol. 467, no. March, p. 143028, 2024, doi: 10.1016/j.jclepro.2024.143028.
[6] Ying H, Guo P, Shen J, Zhang X, Wei Y. Preparation of activated carbon by molten salt electrochemical method and adsorption and recovery on chromium. Ind Crop Prod 2024;222(P3):119814. https://doi.org/10.1016/j.indcrop.2024.119814.
[7] Liu Z, Lu G, Yu J. Electrochemical behavior of magnesium ions in chloride melt. Ionics (kiel) 2019;25(6):2719–27. https://doi.org/10.1007/s11581-019-02881-1.
[8] Wu G, Wang C, Sun M, Ding W. Recent developments and applications on high-performance cast magnesium rare-earth alloys. J Magnes Alloy Jan. 2021;9(1): 1–20. https://doi.org/10.1016/J.JMA.2020.06.021.
[9] Choi M, Lee C, Lee GG, Cho S, Jung J. Technology of molten salt electrolysis of magnesium chloride. Mater Sci Forum 2010;654–656:799–802. https://doi.org/10.4028/www.scientific.net/MSF.654-656.799.
[10] Jeoung H-J, Lee T-H, Yi K-W, Kang J. Review on Electrolytic Processes for Magnesium Metal Production: Industrial and innovative Processes. Mater Trans 2025;66(7):823–39. https://doi.org/10.2320/matertrans.mt-mb2024014.
[11] Wang H, et al. Recovery of lead and iodine from spent perovskite solar cells in molten salt. Chem Eng J 2022;vol. 447, no. May:137498. https://doi.org/10.1016/j.cej.2022.137498.
[12] Tian L, Chen L, Gong A, Wu X, Cao C, Xu Z. Recovery of rare earths, lithium and fluorine from rare earth molten salt electrolytic slag via fluoride sulfate conversion and mineral phase reconstruction. Miner Eng Aug. 2021;170:106965. https://doi.org/10.1016/j.mineng.2021.106965.
[13] Telgerafchi AE, et al. Magnesium production by molten salt electrolysis with liquid tin cathode and multiple effect distillation. Front Chem 2023;11(July):1–13. https://doi.org/10.3389/fchem.2023.1192202.
[14] Lv H, Zhang L, Xi X, Nie Z. Study on separation and purification of titanium alloys (TC4-6Al-4V) by molten salt electrolysis. Sep Purif Technol Feb. 2025;354:129213. https://doi.org/10.1016/j.seppur.2024.129213.
[15] Jiao H, Song WL, Chen H, Wang M, Jiao S, Fang D. Sustainable recycling of titanium scraps and purity titanium production via molten salt electrolysis. J Clean Prod 2020;261:121314. https://doi.org/10.1016/j.jclepro.2020.121314.
[16] Peng C, et al. Eutectic molten salt assisted synthesis of highly defective and flexible ruthenium oxide for efficient overall water splitting. Chem Eng J 2021;vol. 425, no. July:131707. https://doi.org/10.1016/j.cej.2021.131707.
[17] S. qiang Jiao, H. dong Jiao, W. li Song, M. yong Wang, and J. guo Tu, "A review on liquid metals as cathodes for molten salt/oxide electrolysis," *Int. J. Miner. Metall. Mater.*, vol. 27, no. 12, pp. 1588–1598, Dec. 2020, doi: 10.1007/S12613-020-1971-X/METRICS.
[18] Huan S, Wang Y, Peng J, Di Y, Li B, Zhang L. Recovery of aluminum from waste aluminum alloy by low-temperature molten salt electrolysis. Miner Eng Aug. 2020; 154:106386. https://doi.org/10.1016/j.mineng.2020.106386.
[19] Guo B, et al. Sustainable recovery of pure aluminum from scrap aluminum alloy via soluble anode electrolysis: Cathodic deposition behavior of Al and Mg ions in MgCl2–KCl–NaCl molten salt system. J Clean Prod 2025;vol. 521, no. July:146271. https://doi.org/10.1016/j.jclepro.2025.146271.
[20] Guo X, Li H, Yu D, Tian Q. Molten salt electrolysis of spent nickel-based superalloys with liquid cathode for the selective separation of nickel. Sep Purif Technol Dec. 2022;302:122168. https://doi.org/10.1016/j.seppur.2022.122168.
[21] de Figueiredo Luiz D, Boon J, Otero Rodriguez G, van Sint Annaland M. Review of the molten salt technology and assessment of its potential to achieve an energy efficient heat management in a decarbonized chemical industry. Chem Eng J 2024; vol. 498, no. September:155819. https://doi.org/10.1016/j.cej.2024.155819.
[22] U. De Silva and T. P. Coons, "Molten Salt Electrodeposition: Review," *Energies*, vol. 17, no. 15, 2024, doi: 10.3390/en17153832.
[23] Ramakrishnan S, Koltun P. a Comparison of the Greenhouse Impacts of Magnesium Produced by Electrolytic and Pidgeon Processes. Essent Readings Magnes Technol 2016:169–74. https://doi.org/10.1007/978-3-319-48099-2_28.
[24] Pan X-J, Dou Z-H, Zhang T-A, Meng D-L, Fan Y-Y. Separation of metal ions and resource utilization of magnesium from saline lake brine by membrane electrolysis. Sep Purif Technol Nov. 2020;251:117316. https://doi.org/10.1016/j.seppur.2020.117316.
[25] "Magnesium." https://www.essentialchemicalindustry.org/metals/magnesium.html (accessed Sep. 01, 2023).